

Non-homogeneous magnetic field induced magnetic edge states and their transport in a quantum wire

S. M. Badalyan* and F. M. Peeters^o

Department of Physics, University of Antwerp (UIA), B-2610 Antwerpen, Belgium
(October 31, 2018)

Abstract

The spectrum of magnetic edge states and their transport properties in the presence of a perpendicular non-homogeneous magnetic field in a quantum wire formed by a parabolic confining potential are obtained. Systems are studied where the magnetic field exhibits a discontinuous jump in the transverse direction and changes its sign, strength, and both sign and strength at the magnetic interface. The energy spectra and wave functions of these systems, the corresponding group velocities along the interface and the particle average positions normal to the interface are calculated. The resistance of the quantum wire in the presence of such a magnetic interface is obtained both in the ballistic and the diffusive regimes as a function of the Fermi energy and of the homogeneous background magnetic field. The results are compared with those for the case of a homogeneous field.

73.40-c; 73-50-k; 73.23

I. INTRODUCTION

Investigations of reduced dimensionality semiconductor systems is frequently connected with the use of a magnetic field, which, in addition to the lateral confinement, quantizes the carrier motion also in the plane normal to the magnetic field. Particularly, a two-dimensional electron gas (2DEG) exposed to a homogeneous magnetic field has proven to be an extremely rich subject for investigations in theory and experiment¹.

In the last several years a more complex situation of reduced dimensionality semiconductor systems exposed to a *non-homogeneous* magnetic field has attracted considerable interest². Different experimental groups have succeeded in realizing such systems^{3–5}. High mobility 2DEGs are formed in standard GaAs/AlGaAs heterojunctions and the spatial modulation of the magnetic field is achieved by depositing patterned gates of superconducting or ferromagnetic materials on top of the heterostructure. An alternative approach to produce non-homogeneous magnetic fields is by varying the *topography* of an electron gas⁶. These new technologies opened up a new dimension for investigations of reduced dimensionality semiconductor systems. Characterizing and understanding transport properties of these systems are crucial both for fundamental physics and for device applications.

Theoretically the transport properties of reduced dimensionality semiconductor systems subjected to a spatial dependent magnetic field have been addressed in several recent works. The possibilities of the creation of periodic superstructures by a non-homogeneous magnetic field were investigated in Refs. 7–9. The magnetic field dependence of the conductance of a ballistic quantum wire a finite section of which is subjected to a magnetic field¹⁰ and of a 2DEG through an orifice¹¹ was investigated. The single-particle energy spectrum of a 2DEG subjected to a non-homogeneous magnetic field was calculated for different step-like¹², linearly^{13,14}, and parabolically (in the transverse direction of a one dimensional channel)¹⁵ varying with position, and for other functional magnetic field profiles^{16,17}. It has been shown that the spectrum consists of states that propagate normal to the field gradient and have remarkable time-reversal asymmetry¹³ in a linearly varying magnetic field while the spatial distribution of electron and current densities has a rich structure related to the energy quantization¹⁴. Transport properties of a 2DEG in a magnetic superlattice have been investigated in weakly⁹ and strongly¹⁸ modulated magnetic fields normal to the electron sheet. The combined effect⁹ of the spatially periodic electrostatic and magnetic fields of arbitrary shape has been studied^{19,20}. Analysis of the weak localization and calculation of the Hall and magneto-resistivities of the 2DEG in a non-homogeneous magnetic field have been presented^{21–24}.

Recently, different magnetic structures of nanometer scale have been realized experimentally: a magnetic antidot by depositing a superconducting disk on top of a 2DEG^{25,26}, a large amplitude magnetic barriers^{27–33} and structures with a magnetic field alternating in sign³⁴ have been produced by a single or by an array of ferromagnetic lines fabricated on the surface of the heterostructure in hybrid semiconductor/ferromagnet devices. This realization of different magnetic regions in an electron gas with sharp boundaries was a challenge for theoretical studies of the one-particle electronic states (or the magnetic edge states) moving along the magnetic interfaces in quantum waveguides³⁵, quantum dots^{36,37}, and in infinite 2DEGs^{38,39} exposed to a non-homogeneous magnetic field.

The aim of the present paper is to investigate the magnetic edge states and their transport

properties (in the ballistic and diffusive regimes) in a one-dimensional (1D) channel formed by a parabolic confining potential and exposed to a normal non-homogeneous magnetic field. Structures are studied where the magnetic field changes its sign, strength, and both sign and strength at the magnetic interface. Such a system was recently realized experimentally⁴⁰ by depositing a ferromagnetic stripe on top of the electron gas and by applying a background magnetic field normal to the electron gas. Varying the background field results in all the above situations. We calculate rigorously the energy spectrum and the wave functions of these systems by matching the general solutions of the Schrödinger equation at the magnetic interface. The corresponding group velocities along the interface and the particle average position normal to the interface are obtained. Using the results for the spectrum, we calculate the conductance and the conductivity in the ballistic and diffusive regimes.

The paper is organized as follows. In Sec. II we present the method we use to obtain the spectrum. In Sec. III we carry out actual calculations of the energy spectrum and the wave functions, the group velocity along the interface and the particle average position normal to the interface for the three different cases when the magnetic field changes its sign, strength, and both sign and strength at the magnetic interface. We analyze the dependence on the confining potential strength and on the magnetic field strength in one side of the interface while the magnetic field in the other side is kept fixed. In Sec. IV we calculate the conductance and the conductivity in the ballistic and diffusive regimes both as a function of the Fermi energy and of the background magnetic field. The results are compared with those in case of a homogeneous magnetic field. The results are summarized in Sec. V.

II. APPROACH

We investigate the magnetic edge states in a one-dimensional electron channel along the y -direction formed by the parabolic confining potential $V(x)$ and exposed to a normal non-homogeneous magnetic field $B_z(x) = B_1$ and $B_z(x) = -B_2$ respectively on the left and the right hand side of the magnetic interface located at $x = 0$ (see Fig. 1). This system is placed in a homogeneous background magnetic field $B_z(x) = B_b$. Varying the background magnetic field from $-B_b$ to B_b ($B_b > B_1, B_2$) allows to have situations where the effective non-homogeneous magnetic field changes its sign, strength, and both sign and strength at the magnetic interface.

In any finite region along the x -direction where the magnetic field is uniform, the system is described by the single particle Hamiltonian

$$H = \frac{1}{2m^*} \left(\vec{p} + \frac{e}{c} \vec{A} \right)^2 + V(x) \quad (1)$$

where m^* is the particle effective mass, $V(x) = m^* \omega_0^2 x^2 / 2$ the confining potential with ω_0 the confining potential strength. Because of the system translation invariance in the y -direction we choose for the vector potential the Landau gauge $\vec{A} = (0, Bx, 0)$. In this gauge the Schrödinger equation can be separated with the ansatz

$$\Psi(x, y) = e^{iky} \psi(x), \quad (2)$$

where ψ is an eigenstate of the one-dimensional problem

$$\left[\frac{d}{dx^2} + \nu + \frac{1}{2} - \frac{(x - X(k))^2}{4} \right] \psi(x - X(k)) = 0. \quad (3)$$

Here we introduce the following notations: $\nu + \frac{1}{2} = \left(\varepsilon - \frac{\hbar^2 k^2}{2m_B} \right) / \hbar \omega^*$ is the particle transverse energy in units of the oscillator frequency $\omega^* = \sqrt{\omega_B^2 + \omega_0^2}$, ω_B is the cyclotron frequency, ε and k are the energy and the momentum of the particle. The coordinate of the center of orbital rotation is $X(k) = kl^* \omega_B / \omega^*$ in units of the length scale $l^* = \sqrt{\hbar / (m^* \omega^*)}$ related to ω^* . In the longitudinal direction the electron acquires a new field dependent mass $m_B = m^* \omega^{*2} / \omega_0^2$ which is larger than the effective mass m^* . Equation (3) is to be solved under the boundary conditions $\psi(x - X(k)) \rightarrow 0$ when $x \rightarrow \pm\infty$. The solutions are the parabolic cylindrical functions⁴¹

$$D_\nu(x) = -\frac{2^{\frac{1}{2} + \frac{\nu}{2}} \sqrt{\pi} x {}_1F_1\left(\frac{1}{2} - \frac{\nu}{2}, \frac{3}{2}, \frac{x^2}{2}\right)}{e^{\frac{x^2}{4}} \Gamma\left(\frac{-\nu}{2}\right)} + \frac{2^{\frac{\nu}{2}} \sqrt{\pi} {}_1F_1\left(\frac{-\nu}{2}, \frac{1}{2}, \frac{x^2}{2}\right)}{e^{\frac{x^2}{4}} \Gamma\left(\frac{1}{2} - \frac{\nu}{2}\right)}, \quad (4)$$

with ${}_1F_1(a; b; x)$ the Kummer function. For any value of ν there are two independent solutions $D_\nu(x)$ and $D_\nu(-x)$. If $\nu \neq 0, 1, 2, \dots$, then $D_\nu(x) \rightarrow 0$ when $x \rightarrow +\infty$ and $D_\nu(x) \rightarrow \infty$ when $x \rightarrow -\infty$.

In the non-homogeneous magnetic field case ν, X are different on the left and right hand side of the magnetic interface. We construct the wave function as

$$\psi_{\nu_1, \nu_2}(x, X_1, X_2) = \begin{cases} D_{\nu_1}(\sqrt{2}(X_1(k) - x)), & \text{if } x < 0, \\ D_{\nu_2}(\sqrt{2}(x - X_2(k))), & \text{if } x > 0. \end{cases} \quad (5)$$

Indices 1, 2 refer to the values of quantities for which $\omega^* = \sqrt{\omega_B^2 + \omega_0^2}$ is taken with $B = B_1$ and $B = B_2$, respectively. Matching of this wave function and its derivative at $x = 0$ leads to the following dispersion equation

$$\left. \frac{d \ln(D_{\nu_1}(x - X_1(k)))}{dx} \right|_{x=0} = \left. \frac{d \ln(D_{\nu_2}(-x + X_2(k)))}{dx} \right|_{x=0}. \quad (6)$$

By solving this equation we obtain the energy spectrum $\varepsilon_n(k)$ and the wave functions $\psi_{\nu_1, \nu_2}(x, X_1, X_2)$ of the magnetic edge states, which are the solution of the one-dimensional problem with the effective potential

$$V_{eff}(x, k) = \begin{cases} \frac{1}{2} m \omega_1^{*2} (x - X_1(k))^2 + \frac{\hbar^2 k^2}{2m_{B_1}}, & \text{if } x < 0, \\ \frac{1}{2} m \omega_2^{*2} (x - X_2(k))^2 + \frac{\hbar^2 k^2}{2m_{B_2}}, & \text{if } x > 0. \end{cases}$$

The shape of $V_{eff}(x, k)$ depends strongly on the sign of the wave number k and on the magnetic field profile.

III. SPECTRUM

A. Symmetric system: $B_1 = B_2$, $\text{sign}(B_1/B_2) = -1$

In this symmetric case, the dispersion equation (6) breaks into two pieces

$$D_\nu(x - X(k)) = 0, \quad D'_\nu(x - X(k)) = 0 \quad (7)$$

i.e. the zeroes of the parabolic cylindrical function and its derivative give the single particle spectrum of the magnetic edge states. Notice that the first equation gives the spectrum of the usual edge states in a uniform magnetic field for the infinite hard wall confining potential⁴²⁻⁴⁵. First we find the spectrum from the above Eqs. (7) using the asymptotics of the parabolic cylindrical functions and its derivative in the limits of $k \rightarrow \pm\infty$.

In the limit of $k \rightarrow +\infty$ ($x \gg 1, x \gg 2\sqrt{\nu}$) we use the following asymptotic forms for the parabolic cylindrical functions⁴⁶ and its derivative

$$\begin{Bmatrix} D_\nu(-x) \\ D'_\nu(-x) \end{Bmatrix} \sim \begin{Bmatrix} 1 \\ -x \end{Bmatrix} \left[x^\nu \exp\left(i\pi\nu - \frac{x^2}{4}\right) \pm \frac{\sqrt{2\pi}}{\Gamma(-\nu)} x^{-\nu-1} \exp\left(\frac{x^2}{4}\right) \right], \quad (8)$$

and find the energy

$$\varepsilon_n(k) \approx \left(n + \frac{1}{2}\right) \hbar\omega^* + \frac{\hbar^2 k^2}{2m_B} \mp \frac{2^n (kl^*)^{2n+1}}{\sqrt{\pi} n!} \left(\frac{\omega_B}{\omega^*}\right)^{2n+1} \exp\left(-(kl^*)^2 \frac{\omega_B^2}{\omega^{*2}}\right). \quad (9)$$

The corresponding trajectories of the electron orbits have their center of orbital motion located far from the magnetic interface, i.e. $X(k) \gg 1$, but they are on the same side of the magnetic interface where the particle is moving. The energy differs exponentially from the energy of the *hybrid* states of the uniform magnetic field case. Exponentially small interaction between the hybrid states located at a finite distance on both sides of the magnetic interface shifts exponentially small the energy levels up and down with respect to the bare spectrum of the hybrid states of the uniform magnetic field case. The wave function of each level of the magnetic edge states is represented by a curve, which has two peaks. The peaks are situated far from the magnetic interface both in the positive and the negative magnetic field regions and are connected with an exponentially attenuating "tail" of the wave function near the interface. In the two-dimensional case when $\omega_0 \rightarrow 0$, $m_B \rightarrow \infty$ and the particle velocity due to the confining potential becomes zero, the exponential corrections to the energy results in exponentially small velocities of opposite sign for the states shifted up and down in energy. Notice that the exponential corrections in Eq. (9) cannot be obtained from quasiclassical considerations.

In the opposite limit of $k \rightarrow -\infty$ ($\nu \ll 1 - x^2/2\nu \ll 1$) we use the following asymptotic forms for the parabolic cylindrical functions⁴⁶ and its derivative

$$\begin{Bmatrix} D_\nu(x) \\ D'_\nu(x) \end{Bmatrix} \sim \begin{Bmatrix} \sqrt{2} \\ -x \end{Bmatrix} \left(\nu + \frac{1}{2}\right)^{\nu/2} \left(1 - \frac{x^2}{2\nu}\right)^{\mp 1/4} \exp\left(-\frac{\nu}{2} - \frac{1}{4}\right) \quad (10)$$

$$\times \begin{Bmatrix} \cos \\ \sin \end{Bmatrix} \left(\frac{2}{3}\nu \left(1 - \frac{x^2}{2\nu}\right)^{3/2} - \frac{\pi}{4}\right), \quad (11)$$

and find the energy

$$\varepsilon_n(k) \approx \left(n + \frac{1}{2}\right) \hbar\omega^* + \frac{\hbar^2 k^2}{2m^*} + \left(a_n \frac{kl^* \omega_B}{\sqrt{2} \omega^*}\right)^{2/3}, \quad a_n = \frac{3\pi}{2} \left(n - \frac{1}{2} \mp \frac{1}{4}\right). \quad (12)$$

This spectrum characterizes the particle motion in *snake* orbits, i.e. in trajectories whose center of orbital motion are located far from the magnetic interface, i.e. $X(k) \gg 1$, but on the opposite side of the magnetic interface where the particle is moving. To first order in k the confining potential has no influence on the energy along the y -direction and the particle mass is the free electron mass m^* . This is because the effective potential minimum $V_{eff}(x) = \hbar^2 k^2 / 2m^*$ at $x = 0$ does not depend on the confining potential strength ω_0 for negative k (see Fig. 2 where we summarised the three different shapes of the effective 1D potential for the symmetric system).

The exact spectrum, shown in Fig. 3, is described by a discrete quantum number $n = 0, 1, 2, \dots$ and a continuous momentum k . For a given n the energy spectrum exhibits a pronounced asymmetry with respect to positive and negative values of k . The corresponding group velocities v_n along the interface and the particle average semi-thickness Δx_n normal to the interface are shown in Fig. 4 (in this symmetrical system, $B_1 = -B_2$, the particle average position \bar{x}_n is zero, and therefore we calculated the quantity $\Delta x_n = \frac{1}{2} \sqrt{(x - \bar{x}_n)^2}$). It is seen from Figs. 2 and 4 that for large negative values of k , particles are confined in a narrow region around the magnetic interface. The corresponding wave functions are represented by one-peak curves localized near the magnetic interface. These states correspond to the snake orbits, which wiggle around the magnetic interface moving alternatively in the positive and negative magnetic field regions. Since the coordinate of the orbit centrum, $X(k)$, increases with k , the radius of the orbit should also increase to ensure particle motion on the opposite side of the magnetic interface. This requires an increase of the energy with k , and therefore all these snake states acquire a large velocity along the interface, which increases approximately linearly in k while the width Δx_n of the snake orbits decreases in k and reaches its minimum value.

For positive values of k a triangular like barrier is developed at $x = 0$ and the effective potential becomes the double well (see Fig. 2). The height of the barrier is $V_{eff}(x) = \hbar^2 k^2 / 2m^*$ at $x = 0$ while the well minima are $\hbar^2 k^2 / 2m_B$ at $x = \pm X(k)$. For small positive values of k the particle motion is still snake-like around the magnetic interface. The momentum and the velocity of these states have opposite sign. Starting from some value $k_n > 0$ the ground state electron wave functions is split into the two peaks by the barrier. For large positive values of k the spectrum characterizes the exponentially weak coupled two hybrid states located at $x \approx \pm X(k)$ in the positive and negative magnetic field regions and therefore rotate in opposite direction. The velocity of these hybrid states is mainly due to the confining potential and directed opposite to the velocity of the snake states. The absolute value of the velocity is determined by the height of the minima of the effective potential wells, i.e. by the mass m_B which is larger than the free electron mass m^* , therefore the snake states are faster than the hybrid states. For large positive values of k both the group velocities v_n and the particle average semi-thickness Δx_n increase approximately linearly in k (see Fig. 4). The velocity (the average semi-thickness) of the symmetric and anti-symmetric states tend respectively to its asymptotic value $v_n = \hbar k / m_B$ ($\Delta x_n = X$) from above (below) and below (above).

B. Asymmetric system: $B_1 \neq B_2$, $\text{sign}(B_1/B_2) = -1$

The effective potential for this asymmetric system where the magnetic field changes both its strength and sign at the magnetic interface is shown in Fig. 5. In this case the effective potential $V_{eff}(x, k)$ exhibits a pronounced asymmetry both as a function of k and x . For negative values of k , the effective potential is a triangular-like asymmetric well with a minimum of $V_{eff}(x) = \hbar^2 k^2 / 2m^*$ at $x = 0$. For positive values of k the effective potential is a double well with different minima $\hbar^2 k^2 / 2m_{B_1}$ and $\hbar^2 k^2 / 2m_{B_2}$ at the positions $x = +X_1(k)$ and $x = -X_2(k)$, respectively. The triangular like barrier between the wells has again the height $V_{eff}(x) = \hbar^2 k^2 / 2m^*$ at $x = 0$. Thus the confining potential together with the non-homogeneous magnetic field induces three effective masses (m^* for negative and m_{B_1} , m_{B_2} for positive values of k) in the system. For negative values of k , the spectrum corresponds to snake orbits with free-like motion and with mass m^* along the y -direction (see Fig. 6). These states are effectively localized in the vicinity of the magnetic interface in the region where the magnetic field is smaller and the magnetic length is larger. The group velocity is approximately linear (see Fig. 7) and the particle average position \bar{x}_n is approximately independent of the wave number (see Fig. 8). The $n = 1$ level is the closest to the magnetic interface and most remote from the $n > 1$ states. For positive k the spectrum characterizes the hybrid states with two different masses m_{B_1} and m_{B_2} . Each energy band n has n anti-crossings with these hybrid states. For some positive value of k the group velocity v_n and the particle average position \bar{x}_n start to oscillate as a function of the wave number and the particle tunnels periodically from the left to the right side of the quantum wire and vice versa (see Fig. 8). At $k \rightarrow +\infty$ all states tend to be localized in the region where the magnetic field is large and the well of the effective potential is lower. Contrary to the symmetric system, the ground state wave function consists now of a curve with one peak. At the anti-crossing points the wave function changes sign and its peak position shifts rapidly by changing its sign and value (see Fig. 9). This corresponds to a tunneling of the particle from the one well of the effective potential to the other. This picture is true even if there is only a small difference between the magnetic field on both sides of the interface, which brakes the symmetry of the system and the particle is forced to choose one of the wells.

C. Asymmetric system: $B_1 \neq B_2$, $\text{sign}(B_1/B_2) = 1$

In such systems in which at the magnetic interface the magnetic field changes only its strength, the effective potential consists of only one well (see Fig. 10). For negative values of k the well is located at $x = -X_2(k)$ with minimum value $\hbar^2 k^2 / 2m_{B_2}$. It is higher and broader than the well for positive values of k with minimum $\hbar^2 k^2 / 2m_{B_1}$ at the position $x = +X_1(k)$ ($B_1 > B_2$). There are no snake states in this system and the spectrum for both large negative and positive values of k characterizes hybrid states with masses m_{B_2} and m_{B_1} (Fig. 11). These states rotate in the same direction on both sides of the magnetic interface and their group velocities have opposite sign. Both the velocity and the particle average position of any level n are approximately linear in k for large negative and positive k and tend respectively to their asymptotic values $v_n = \hbar k / m_{B_2}$, $\bar{x}_n = -X_2(k)$ and $v_n = -\hbar k / m_{B_1}$, $\bar{x}_n = X_1(k)$, which are independent of n (see Fig. 12). For intermediate values of k the velocity and the particle average position exhibit smooth oscillations as a function of k .

For these values of k the corresponding states are confined in the effective potential which consists of two partial parabolas with different strengths. With varying k the influence of each parabola changes strongly in contributing to these states.

D. Dependence on the confining potential strength

In Figs. 13 (a-d) the dependence of the energy on the confining potential frequency ω_0 is depicted when $B_1 = -3B_2$ and $B_1 = 3B_2$ both for $kl^* = \pm 2$. It is seen that there is a strong asymmetry with respect to the sign of the magnetic field and of the wave number. For the systems where the magnetic field changes its sign and strength at the magnetic interface, the states with $kl^* = -2$ correspond to snake orbits. In this case the dependence on ω_0 is very weak because the effective potential consists of only one well with minimum value $V(0) = \hbar^2 k^2 / 2m^*$, as we mentioned above, which does not depend on ω_0 . Varying ω_0 changes only the sharpness of the banks of the potential well, which results in a much weaker dependence of the energy bands on k . In the case of $kl^* = +2$ (this corresponds to the region of two hybrid states with different masses m_{B_1} and m_{B_2}) the energy strongly depends on ω_0 . For $\omega_0 = 0$ we have a two-dimensional system^{38,39} and some states are very close in energy due to the special choice of the ratio of the two magnetic fields B_1/B_2 which is an integer. For small values of ω_0 , the energy increases strongly with ω_0 . Several anti-crossings appear between the energy bands with different n for this choice of parameters. With further increase of ω_0 the increase of energy becomes weaker and the simple oscillatory states with $B_{1,2} \approx 0$ correspond to the limit $\omega_0/\omega_B \gg 1$.

In the systems where the magnetic field changes only its strength at the magnetic interface, both $kl^* = +2$ and $kl^* = -2$ correspond to hybrid states on the left and right side of the interface, respectively, and the energy dependence on ω_0 is qualitatively similar for these states. The quantitative difference is a result of the different values of the masses m_{B_1} and m_{B_2} (e.g. $m_{B_1}/m_{B_2} = 45/13$ for $\omega_{B_1} = 2\omega_0 = 3\omega_{B_2}$). It is easy to see that for $\omega_0 = 0$ the energy takes values near $1/6, 1/2, 5/6, \dots$ if $kl^* = -2$ and $1/2, 3/2, 5/2, \dots$ if $kl^* = +2$ as it should be for a two-dimensional system^{38,39}.

E. Dependence on the magnetic field B_2

In Figs. 14 (a,b) we plot the energy dependence on the magnetic field B_2 for fixed B_1 and for the confining potential frequency $\omega_0/\omega_{B_1} = 1/2$ for $kl^* = \pm 2.25$. Notice there is a strong asymmetry with respect to the sign of k . When $kl^* = -2.25$ the energy dependence on B_2 for negative B_2 is weaker than for positive B_2 because in the first range the spectrum characterizes the snake states and the dependence on B_2 is mainly due to the dependence of ω_2^* on B_2 while in the second range the spectrum characterizes the hybrid states and the energy dependence is due to the dependence of both ω_2^* and m_{B_2} on B_2 . It is easy to see that for $B_2/B_1 = \pm 1, \pm 1/3$ the energy values are consistent with that in Figs. 3, 6, and 11.

For $kl^* = +2.25$ the first energy level almost does not depend on B_2 . For positive values of B_2 the spectrum describes only the hybrid states and for the chosen large value of $kl^* = +2.25$ the energy equals approximately its asymptotic value, $\hbar\omega_1^*/2 + \hbar^2 k^2 / 2m_{B_1}$, which is independent of B_2 . For negative values of B_2 , the energy is again approximately

those of the hybrid states with the same energy because $kl^* = +2.25$ is larger than the value k_1l^* at which the ground state exhibits an anti-crossing. Analogous behavior is found for the second energy level, but now starting from some negative value of B_2 this level, after anti-crossing with the level $n = 3$, tends to the first level because of the degeneracy of the symmetric and anti-symmetric terms in the $B_1 = -B_2$ symmetric system (see Fig. 3). For $B_2 < -B_1$, the degeneracy is lifted and the energy increases with $|B_2|$.

IV. TRANSPORT

We calculate the zero temperature two terminal magneto-conductance for a perfect conductor using the Büttiker formula⁴⁷

$$G(E_F) = \frac{2e^2}{\hbar} N(E_F), \quad (13)$$

where $N(E)$ is the number of magnetic edge states with energy E and positive velocity. From Fig. 15 it is seen that the conductance, in the ballistic regime and for different magnetic field profiles, exhibits stepwise variations as a function of the Fermi energy. For a given energy and confining potential strength, the conductance in the non-homogeneous magnetic field is nearly twice that for the homogeneous field case. The conductance decreases when going from the profile $B_1 = -3B_2$ to the profiles $B_1 = -B_2$, and $B_1 = +3B_2$. For the symmetric profile the narrow plateau is followed by broad ones. This asymmetry is not visible for the other profiles. The conductance is the same in the positive and negative directions along the magnetic interface despite the strong asymmetry in the magnitude of the velocity of the states moving in opposite directions.

The conductivity in the diffusive regime is calculated in the relaxation time approximation

$$\sigma_{1D} = \frac{e^2}{L} \sum_{n,k} v_n^2(k) \tau(\varepsilon) \left(-\frac{\partial f_T}{\partial \varepsilon} \right), \quad (14)$$

where L is the length of the quantum wire, τ is the momentum relaxation time, f_T is the Fermi-Dirac distribution function at temperature T . We calculate the conductivity in the zero temperature limit. Then the derivative of the Fermi function is a δ -function. Replacing all quantities in Eq. (14) by their values at the Fermi energy, we obtain

$$\sigma_{1D} = \frac{2e^2}{h} \tau(E_F) \sum_n |v_n(k)| \Big|_{\varepsilon=E_F}. \quad (15)$$

In the diffusive regime, we have calculated separately the conductivity due to states with negative and positive velocities as a function of the Fermi energy for the two magnetic field profiles, $B_1 = -3B_2$ and $B_1 = +3B_2$ (see Fig. 16). In both cases the conductivity due to states with negative velocities (dashed curves) is larger than that due to states with positive velocities (dotted curves). In the case when the magnetic field changes its sign, the states with negative velocities are the snake states, which are always faster than the states with positive velocities which are related to the hybrid states. In the case of $B_1 = +3B_2$ all the

states are hybrid states, however, the contribution to the conductivity of the states with negative velocities is larger because these states are located in a region with small magnetic field, have the small mass m_B , and large velocity v_n . For both $v_n > 0$ and $v_n < 0$ parts, the conductivity has an oscillating structure as a function of the Fermi energy which is due to a divergence of the density of states at the bottom of the $\varepsilon_n(k)$ band. However, the contributions due to states with $v_n > 0$ exhibit an additional structure related to the oscillations of the group velocity as a function of k . This structure is more pronounced in the case of $B_1 = -3B_2$, the conductivity has additional distinct minima that reflect the tunneling effect discussed above. Notice that the conductivity of the system with the magnetic field profile $B_1 = -3B_2$ is roughly 1.5 times larger than that for the field profile $B_1 = +3B_2$.

In Fig. 17 the magnetic depopulation diagram is plotted as a function of the background magnetic field B_b and the wave number k for the initial magnetic field profile $B_1 = 2B_0 = -3B_2$ (B_0 is the resonance field for which $\omega_0 = \omega_{B_0}$) and for the Fermi energy $E_F = 5\hbar\omega_1^*$. In the shaded region the effective magnetic field changes its sign at the magnetic interface. At the background magnetic field $B_b = 0$ there are 18 current carrying states represented by the solid dots in the figure. The left 9 symbols correspond to snake states while the right 9, to hybrid states with both m_{B_1} and m_{B_2} masses. The maximum number of current carrying states, 20, is achieved in the small region of the background magnetic field around $B_{sym} = -2/3B_0$ where the effective magnetic field on both sides of the magnetic interface has equal strength, $4/3B_0$, and opposite sign. The background magnetic field dependence is symmetric with respect to this point. Out of the shaded region the current carrying states are only the hybrid states. At the edges of the shaded region, the effective magnetic field becomes zero on either the left or the right side of the magnetic interface. When the absolute value of the background magnetic field increases starting from the value B_{sym} , the number of current carrying states decreases monotonically.

In Figs. 18 and 19 we plot the magneto-resistance as a function of the background magnetic field in the ballistic and diffusive regimes, respectively, for the situation corresponding to Fig. 17. The resistance in the ballistic regime exhibits stepwise variations as a function of B_b and has a minimum at $B_b = B_{sym}$, which is shifted with respect to the minimum of the resistance in the homogeneous magnetic fields (thin dashed curve). In the later case the dependence on B_b is stronger because the number of current carrying states is smaller. In the diffusive regime the resistance exhibits small peaks as a function of B_b that are associated with the magnetic depopulation effect and that are on top of a positive magneto-resistance background, which increases with B_b when B_b has the same sign as the initial magnetic field of the region where the magnetic field is larger. For small values of B_b the resistance in the homogeneous field is smaller. The slope of the resistance variation in B_b in the homogeneous field case is larger than for non-homogeneous fields. Notice that the minima of the conductivity due to the hybrid states with $v_n > 0$ associated with the tunneling effect (see Fig. 16) are not visible in the background magnetic field dependence of the resistance in Fig. 19. This is possibly due to the special choice of the initial parameters ($B_1 = 2B_0 = -3B_2$) and of the Fermi energy, the possible peak values of the resistance are out of the small range of the variation of B_b (from 0 to $2/3B_0$) where the effective magnetic field changes its sign. Moreover, the effective magnetic field on one side of the magnetic interface is given by $-B_2 + B_b$, i.e. the increase of the background magnetic field diminishes the effective

magnetic field, namely in the region where the initial magnetic field is smaller

V. SUMMARY

We developed a theory for the non-homogeneous magnetic field induced magnetic edge states and their transport in a quantum wire formed by a parabolic confining potential. We studied systems in which the magnetic field perpendicular to the wire axis exhibits a discontinuous jump in the transverse direction and changes its sign, strength, and both sign and strength at the magnetic interface. The energy spectrum and the wave functions of the magnetic edge states were calculated by matching the general solutions of the Schrödinger equation at the magnetic interface. The corresponding group velocities along the interface and the particle average position normal to the interface were obtained.

The spectrum consists of alternating symmetrical and anti-symmetrical terms and is described by a discrete quantum number $n = 0, 1, 2, \dots$ and the momentum k along the wire. For given n the energy spectrum exhibits a pronounced asymmetry with respect to positive and negative values of k and describes snake orbits and hybrid states. Contrary to two-dimensional systems^{38,39}, the confining potential together with the non-homogeneous magnetic field induces three effective masses, which can account for most of the system properties. When the magnetic field changes its sign and strength, all states with negative momenta (the snake orbits) are effectively localized in the vicinity of the magnetic interface in the region where the magnetic field is small. The group velocity is approximately linear and the particle average position is approximately independent of the momentum. For a positive momentum the spectrum exhibits anti-crossings, the group velocity and the particle average position oscillate as a function of the momentum and the particle tunnels periodically from the left to the right side of the quantum wire and vice versa. At $k \rightarrow +\infty$ all states tend to be localized in the region where the magnetic field is large.

The conductance in the ballistic regime exhibits stepwise variations as a function of the Fermi energy and of the background magnetic field. For a given energy and confining potential strength, the conductance in the non-homogeneous magnetic field is nearly twice that in the case of a homogeneous field. The conductance has a maximum as a function of B_b at the value for which the effective magnetic field on the left and on the right hand side of the magnetic interface has the same strength and opposite sign.

In the diffusive regime, we calculated separately the conductivity for negative and positive velocities as a function of the Fermi energy and the background magnetic field B_b . The conductivity due to states with negative velocities is large. The conductivity oscillates as a function of the Fermi energy. The contributions due to states with positive velocities exhibit an additional structure related to the oscillations of the group velocity as a function of k . In the systems where the magnetic field changes its sign this structure is more pronounced with additional distinct minima related to the tunneling of the particle between different magnetic regions. The resistance exhibits small peaks as a function of background magnetic field that are associated with magnetic depopulation effects.

ACKNOWLEDGEMENT

This work was partially supported by the Flemish Science Foundation (FWO-VI), the Inter-university Micro-Electronic Center (IMEC, Leuven), the "Onderzoeksraad van de Universiteit Antwerpen", and the IUAP-IV (Belgium). S. M. B. was supported by a DWTC-fellowship to promote the S & T collaboration with Central and Eastern Europe and a CRDF grant No 375100. We acknowledge fruitful discussions with J. Reijniers.

REFERENCES

- * Permanent address: Department of Radiophysics, Yerevan State University, 375049 Yerevan, Armenia
- ^o Electronic mail: peetersuia.ua.ac.be
- ¹ *High Magnetic Fields in Semiconductor Physics III*, edited by G. Landwehr (Springer-Verlag, Berlin Heidelberg, 1992).
- ² F. M. Peeters and J. De Boeck, in *Handbook of nanostructured materials and technology*, edited by N. S. Nalwa, Vol. 3 (Academic Press, N. Y., 1999), p. 345.
- ³ P. D. Ye, D. Weiss, R. R. Gerhardts, M. Seeger, K. von Klitzing, K. Eberl, and H. Nickel, *Phys. Rev. Lett.* **74**, 3013 (1995).
- ⁴ S. Izawa, S. Katsumoto, A. Endo, and Y. Iye, *J. Phys. Soc. Jpn.* **64**, 706 (1995).
- ⁵ H. A. Carmona, A. K. Geim, A. Nogaret, P. C. Main, T. J. Foster, M. Henini, S. P. Beaumont, and M. E. Blamire, *Phys. Rev. Lett.* **74**, 3009 (1995).
- ⁶ C. L. Foden, M. L. Leadbeater, J. H. Burroughes, and M. Pepper, *J. Phys.: Cond. Matt.* **6**, L127 (1994).
- ⁷ B. A. Dubrovin and S. P. Novikov, *Sov. Phys. JETP* **52**, 511 (1980).
- ⁸ P. P. Vil'ms and M. V. Éntin, *Sov. Phys. Semicond.* **22**, 1209 (1988).
- ⁹ F. M. Peeters and P. Vasilopoulos, *Phys. Rev. B* **47**, 1466 (1993).
- ¹⁰ H. Yoshioka, *J. Phys. Soc. Jpn.* **59**, 2884 (1990).
- ¹¹ Y. Avishai and Y. B. Band, *Phys. Rev. B* **40**, 3429 (1989).
- ¹² F. M. Peeters and A. Matulis, *Phys. Rev. B* **48**, 15 166 (1993).
- ¹³ J. E. Müller, *Phys. Rev. Lett.* **68**, 385 (1992).
- ¹⁴ E. Hofstetter, J. M. C. Taylor, and A. MacKinnon, *Phys. Rev. B* **53**, 4676 (1996).
- ¹⁵ Y. Takagaki and K. Ploog, *Phys. Rev. B* **53**, 3885 (1996).
- ¹⁶ M. Calvo, *Phys. Rev. B* **48**, 2365 (1993).
- ¹⁷ A. Matulis, F. M. Peeters, and P. Vasilopoulos, *Phys. Rev. Lett.* **72**, 1518 (1994).
- ¹⁸ I. S. Ibrahim and F. M. Peeters, *Phys. Rev. B* **52**, 17 321 (1995).
- ¹⁹ R. R. Gerhardts, *Phys. Rev. B* **53**, 11064 (1996).
- ²⁰ S. D. M. Zwerschke, A. Manolescu, and R. R. Gerhardts, *Phys. Rev. B* **60**, 5536 (1999).
- ²¹ J. Rammer and A. L. Shel'nikov, *Phys. Rev. B* **36**, 3135 (1987).
- ²² A. V. Khaetskii, *J. Physics Cond. Matt.* **3**, 5115 (1991).
- ²³ L. Brey and H. A. Fertig, *Phys. Rev. B* **47**, 15 961 (1993).
- ²⁴ A. A. Bykov, G. M. Gusev, J. R. Leite, A. K. Bakarov, N. T. Moshegov, M. Casse, D. K. Maude, and J. C. Portal, *Phys. Rev. B* **61**, 5505 (2000).
- ²⁵ A. K. Geim, I. V. Grigorieva, S. V. Dubonos, J. G. S. Lok, J. C. Maan, A. E. Filipov, and F. M. Peeters, *Nature* **390**, 259 (1997).
- ²⁶ A. Smith R. Taboryski, L. T. Hansen, C. B. Sorensen, P. Hedegard, and P. E. Lindelof, *Phys. Rev. B* **50**, 14726 (1994).
- ²⁷ M. Jonson, B. R. Bennett, M. J. Yang, M. M. Miller, and B. V. Shanabrook, *Appl. Phys. Lett.* **71**, 974 (1997).
- ²⁸ F. G. Monzon, M. Jonson, and M. L. Roukes, *Appl. Phys. Lett.* **71**, 3087 (1997).
- ²⁹ J. Reijniers and F. M. Peeters, *Appl. Phys. Lett.* **73**, 357 (1998).
- ³⁰ J. Reijniers and F. M. Peeters, *J. Appl. Phys.* **87**, 8088 (2000).
- ³¹ V. Kubrak, F. Rahman, B. L. Gallagher, P. C. Main, M. Henini, C. H. Marrows, and M. A. Howson, *Appl. Phys. Lett.* **74**, 2507 (1999).

- ³² T. Vančura, T. Ihn, S. Broderick, K. Ensslin, W. Wegscheider, and M Bichler, Phys. Rev. B **62**, 5074 (2000).
- ³³ V. Kubrak A. C. Neumann, B. L. Gallagher, P. C. Main, M. Henini, C. H. Marrows, and M. A. Howson, Physica E **6**, 755 (2000).
- ³⁴ A. Nogaret S. Carlton, B. L. Gallagher, P. C. Main, M. Henini, R. Writz, R. Newbury, M. A. Howson, and S. P. Beaumont, Phys. Rev. B **55**, R16037 (1997).
- ³⁵ B. Y. Gu, W. D. Sheng, X. H. Wang, and J. Wang, Phys. Rev. B **56**, R13434 (1997).
- ³⁶ H. S. Sim, K. H. Ahn, K. J. Chang, G. Ihm, N. Kim, and S. J. Lee, Phys. Rev. Lett. **80**, 1501 (1998).
- ³⁷ J. Reijnders, F. M. Peeters, and A. Matulis, Phys. Rev. B **59**, 2817 (1999).
- ³⁸ F. M. Peeters, J. Reijnders, S. M. Badalian, and P. Vasilopoulos, Microelectronic Engineering **74**, 405 (1999).
- ³⁹ J. Reijnders and F. M. Peeters, J. Phys.: Cond. Matt. (2000).
- ⁴⁰ S. J. A. Nogaret, Bending, and M. Henini, Phys. Rev. Lett. **84**, 2231 (2000).
- ⁴¹ M. Abramowitz and I. A. Stegun, *Handbook of Mathematical Functions* (Nauka, Moscow, 1979), p. 494.
- ⁴² E. A. Kaner, N. M. Makarov, and I. M. Fuks, Sov. Phys. JETP **28**, 483 (1969).
- ⁴³ R. B. Laughlin, Phys. Rev. B **23**, 5632 (1981).
- ⁴⁴ B. I. Halperin, Phys. Rev. B **25**, 2185 (1982).
- ⁴⁵ A. H. MacDonald and P. Středa, Phys. Rev. B **29**, 1616 (1984).
- ⁴⁶ E. M. Gyuninnen and G. I. Makarov, in *Problems of Diffraction and Propagation of Waves*, edited by E. M. Gyuninnen (Leningrad State University Press, Leningrad, 1962), Vol. 1, p. 24.
- ⁴⁷ M. Büttiker, Phys. Rev. B **38**, 9375 (1988).

FIGURES

FIG. 1. Schematic diagram of the system under study. The quantum wire is formed along the y -axis by a parabolic confining potential $V(x) = m^* \omega_0^2 x^2 / 2$ in the x -direction. In the z -direction a non-homogeneous magnetic field $B_z = B_1$ and $B_z = -B_2$ is applied respectively on the left and the right hand side of the magnetic interface at $x = 0$. A homogeneous background magnetic field, $B_z = B_b$, can be additionally applied. The channel width is W , the length scale $l_0^2 = \hbar / (m^* \omega_0)$ is related to the confining potential strength ω_0 , m^* is the electron effective mass, E_F and k_F are the Fermi energy and momentum, respectively.

FIG. 2. The effective potential $V_{eff}(x, k)$ for the symmetric $B_1 = -B_2$ magnetic field profile. The classical trajectories are shown schematically for the snake orbits ($k = 0, -1.5$) and for the hybrid states ($k = 1.5$).

FIG. 3. The energy spectrum for the 8 lowest bands corresponding to the situation of Fig. 2.

FIG. 4. The group velocity along the magnetic interface (the thin curves, the right and top axes) and the particle average semi-thickness (the thick curves, the left and bottom axes) corresponding to Fig. 3.

FIG. 5. The effective potential $V_{eff}(x, k)$ for the asymmetric $B_1 = -3B_2$ magnetic field profile. $V_{eff}(x, k)$ is a single well for $k < 0$ and a double well for $k > 0$. All wells have different widths and are shifted up for different heights determined by the masses m^* , m_{B_1} , and m_{B_2} . The classical trajectories are shown schematically for the snake orbits ($k = 0, -1.5$) and for the hybrid states ($k = 1.5$).

FIG. 6. The energy spectrum for the 8 lowest bands corresponding to the situation of Fig. 5. Each energy band n has n anti-crossings. The symbols (solid dots) correspond to the classical trajectories for $k = 1.5$ in Fig. 5.

FIG. 7. The group velocity along the magnetic interface corresponding to Fig. 6. There are three preferential directions in this figure, θ and θ_1, θ_2 , which define the asymptotic velocities of the snake orbits and hybrid states with the masses m^* and m_{B_1}, m_{B_2} , respectively. The symbols correspond to the classical trajectories for $k = 1.5$ in Fig. 5.

FIG. 8. The particle average position normal to the magnetic interface corresponding to the 5 lowest energy bands in Fig. 6. The symbols correspond to the classical trajectories for $k = 1.5$ in Fig. 5.

FIG. 9. The particle wave functions corresponding to the 2 lowest energy bands in Fig. 6 for several values of the wave number k for $n = 1$ (a) and $n = 2$ (b).

FIG. 10. The effective potential $V_{eff}(x, k)$ for the asymmetric magnetic field profile $B_1 = +3B_2$. $V_{eff}(x, k)$ is always a single well with different heights and widths for $k < 0$ and $k > 0$. The classical trajectories for the hybrid states at $k = 0, \pm 1.5$ are shown schematically.

FIG. 11. The energy spectrum for the 7 lowest bands corresponding to the situation of Fig. 10.

FIG. 12. The group velocity along the magnetic interface (the thick curves, the right and top axis) and the particle average position (the thin curves, the left and bottom axis) corresponding respectively to the 7 and 5 lowest energy bands in Fig. 11.

FIG. 13. The dependence of the energy on the confining potential strength for different magnetic field profiles and for different values of the wave number.

FIG. 14. The dependence of the energy on the magnetic field B_2 for fixed B_1 and for different values of the wave number.

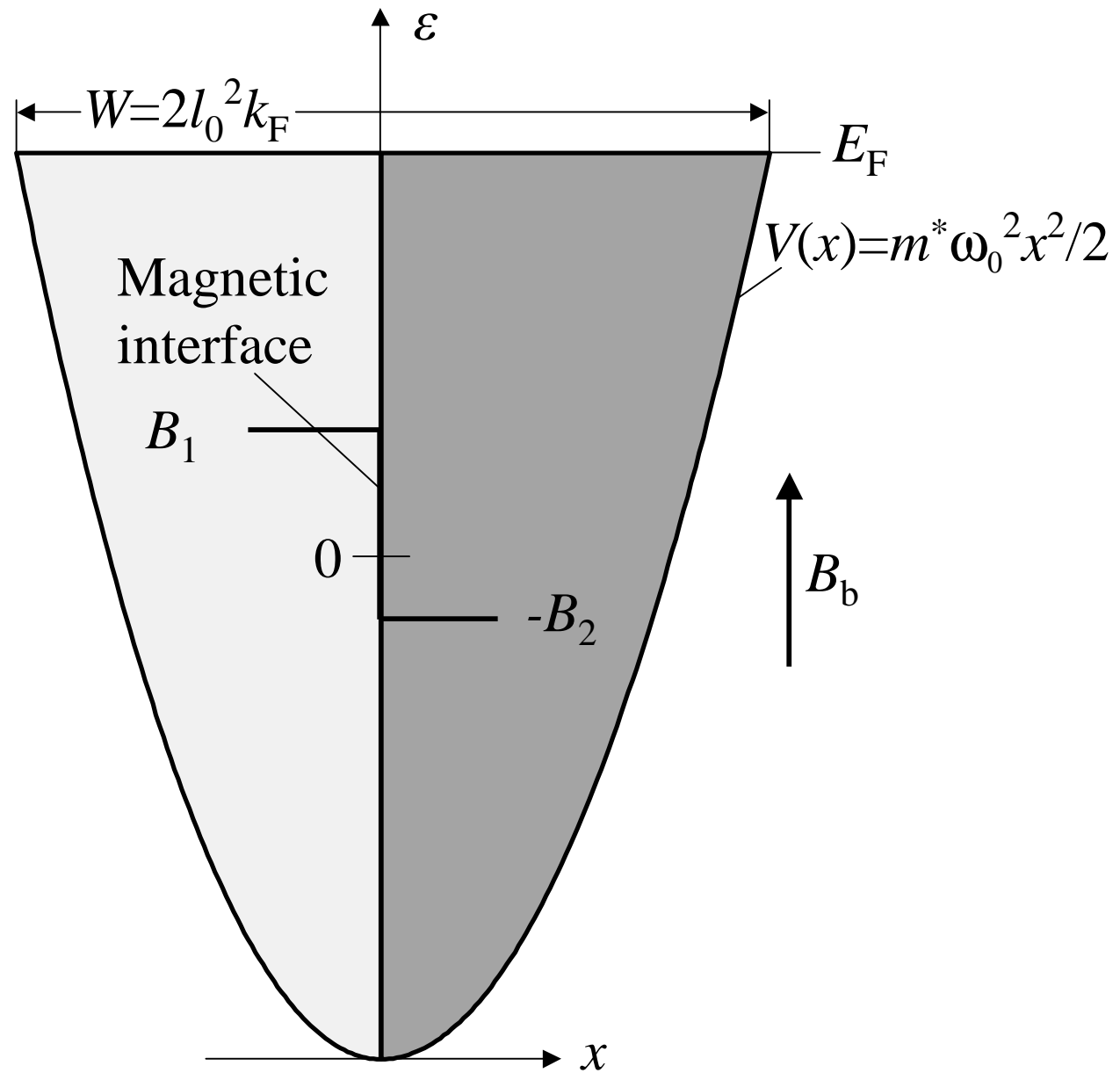
FIG. 15. Dependence of the conductance on the Fermi energy in the ballistic regime for different magnetic field profiles and for fixed confining potential strength.

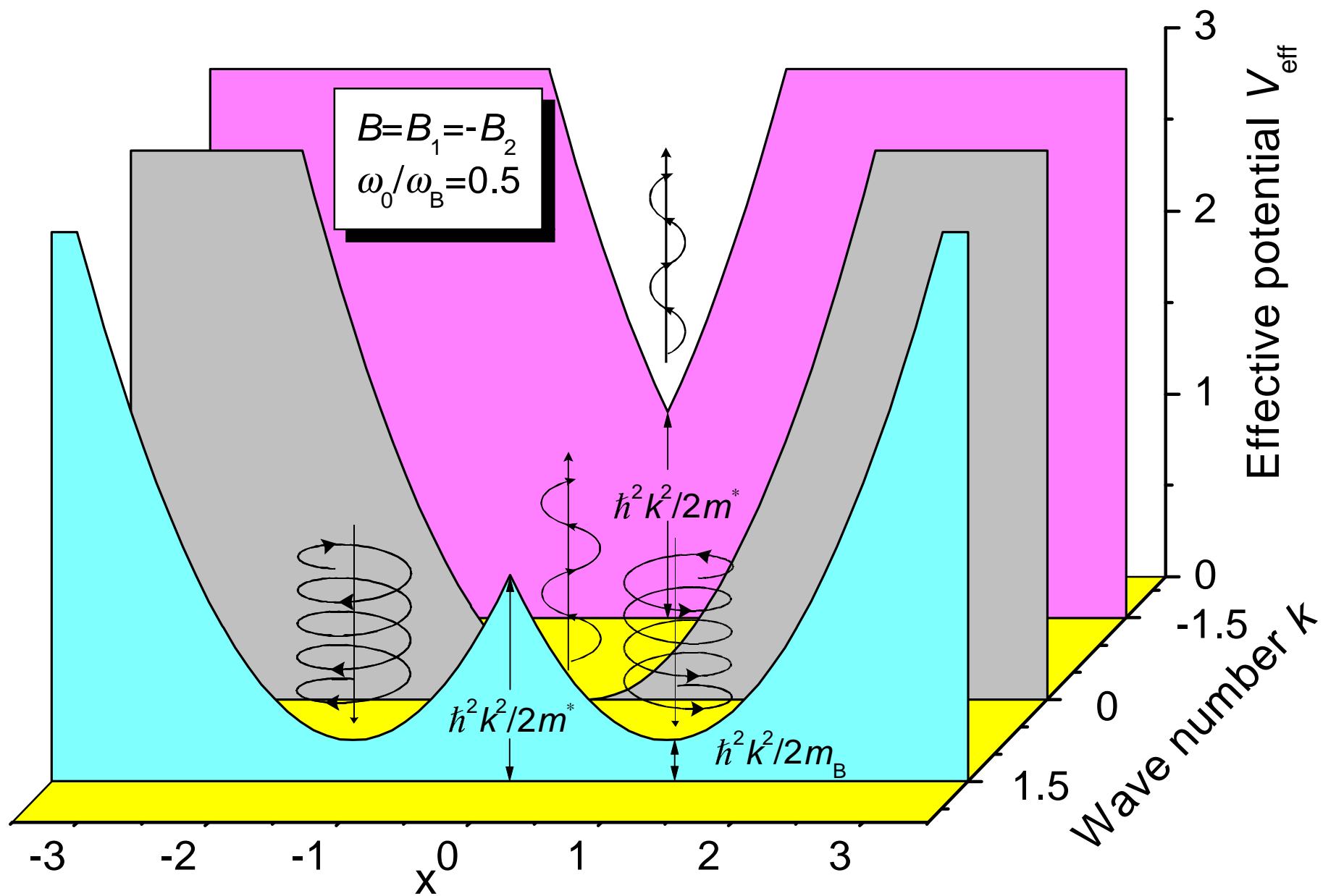
FIG. 16. Dependence of the conductivity, in units of $\sigma_0 = e^2\tau/(\pi m^*l^*)$, on the Fermi energy in the diffusive regime for different magnetic field profiles and for fixed confining potential strength. The contributions to the conductivity of the states with positive and negative velocity are shown separately.

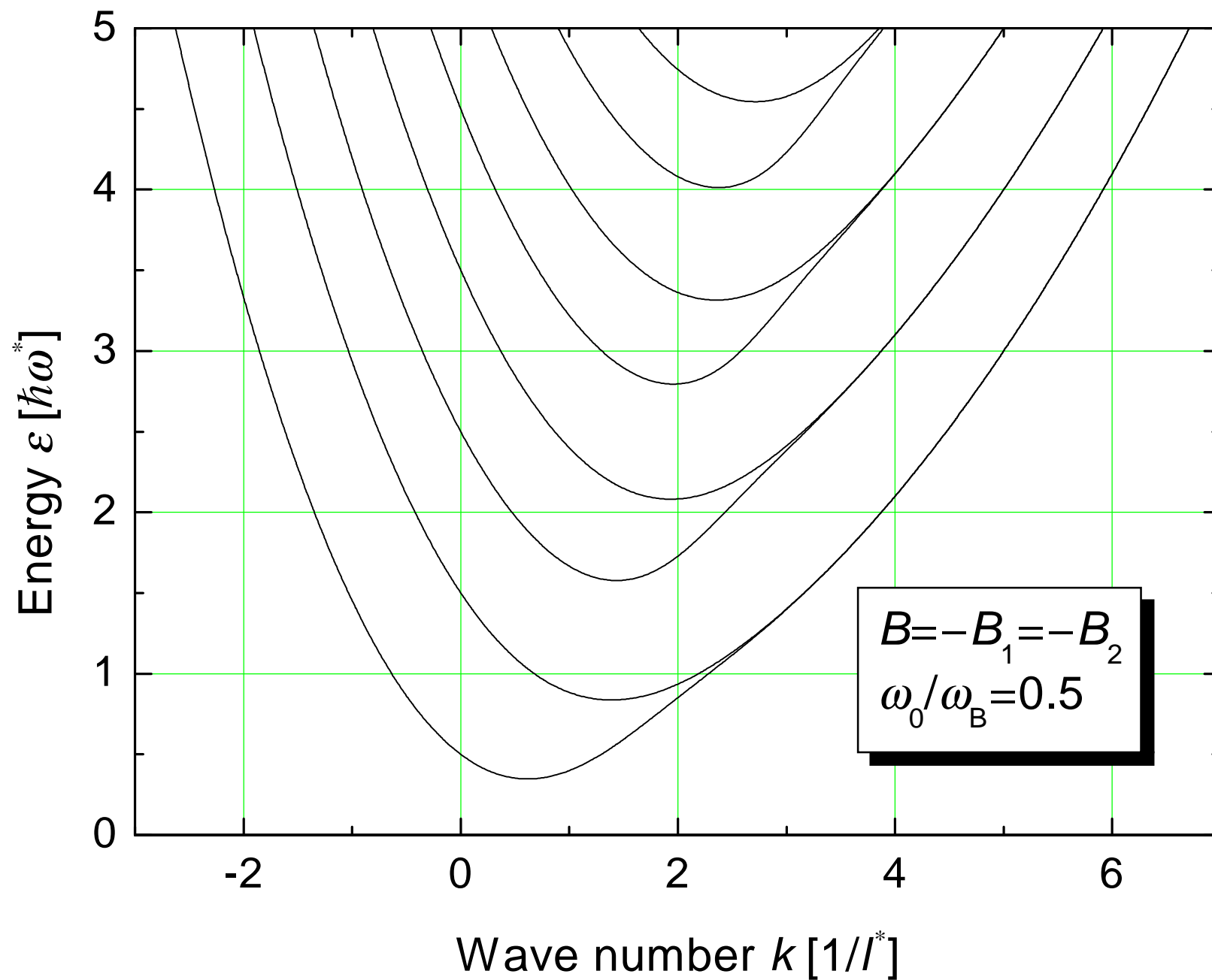
FIG. 17. The magnetic depopulation diagram as a function of the background magnetic field and the wave number for the initial magnetic field profile $B_1 = -3B_2$ and for a fixed Fermi energy $E_F = 5\sqrt{5}\hbar\omega_0$, $l_0^2 = \hbar/(m^*\omega_0)$. The solid dots correspond to the current carrying states at $B_b = 0$. The shaded region corresponds to systems where the effective magnetic field changes its sign at the magnetic interface.

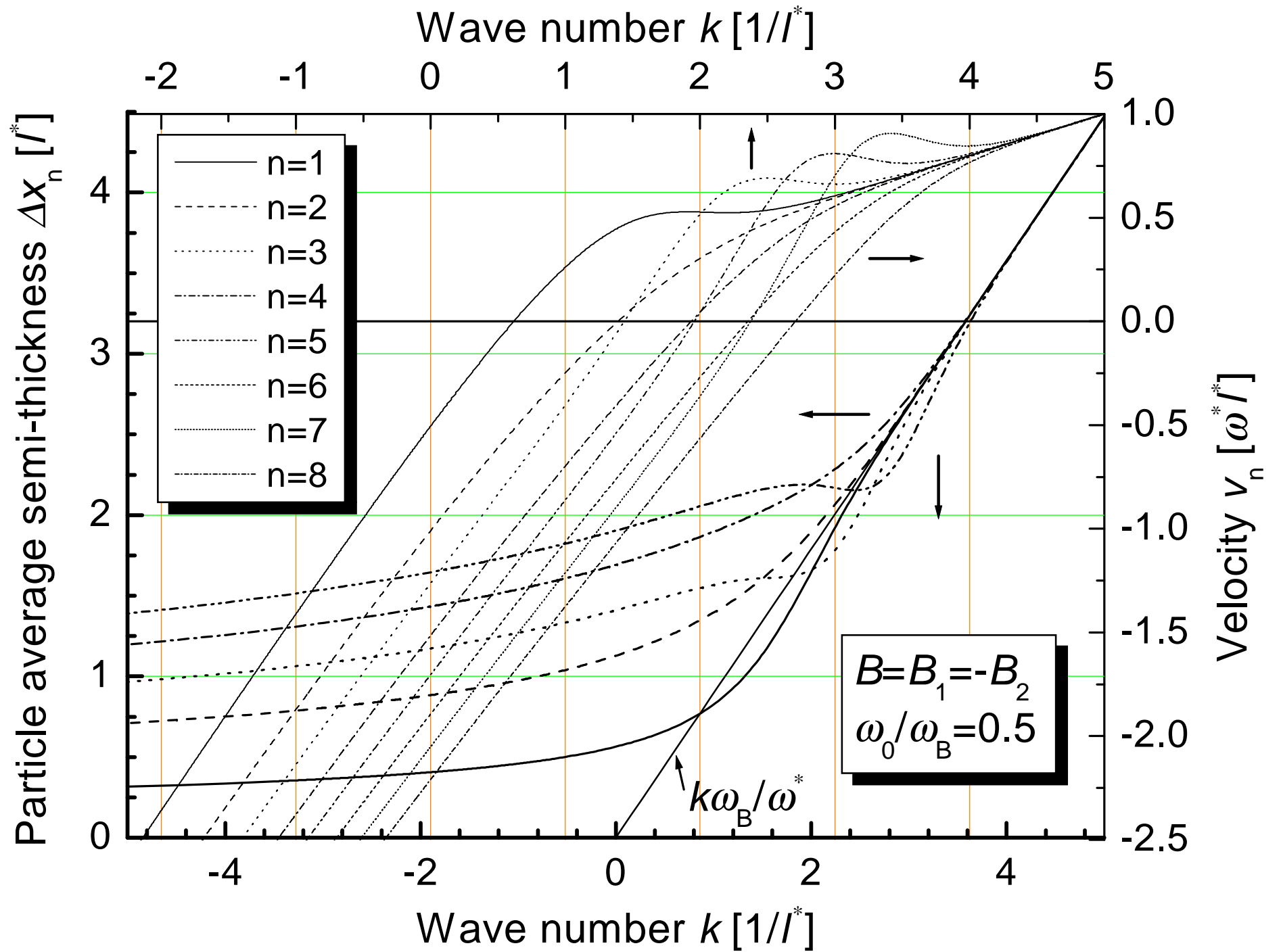
FIG. 18. Dependence of the resistance on the background magnetic field in the ballistic regime for the $B_1 = -3B_2$ initial magnetic field profile and a fixed Fermi energy $E_F = 5\sqrt{5}\hbar\omega_0$. The resistance in case of a homogeneous magnetic field is plotted for comparison.

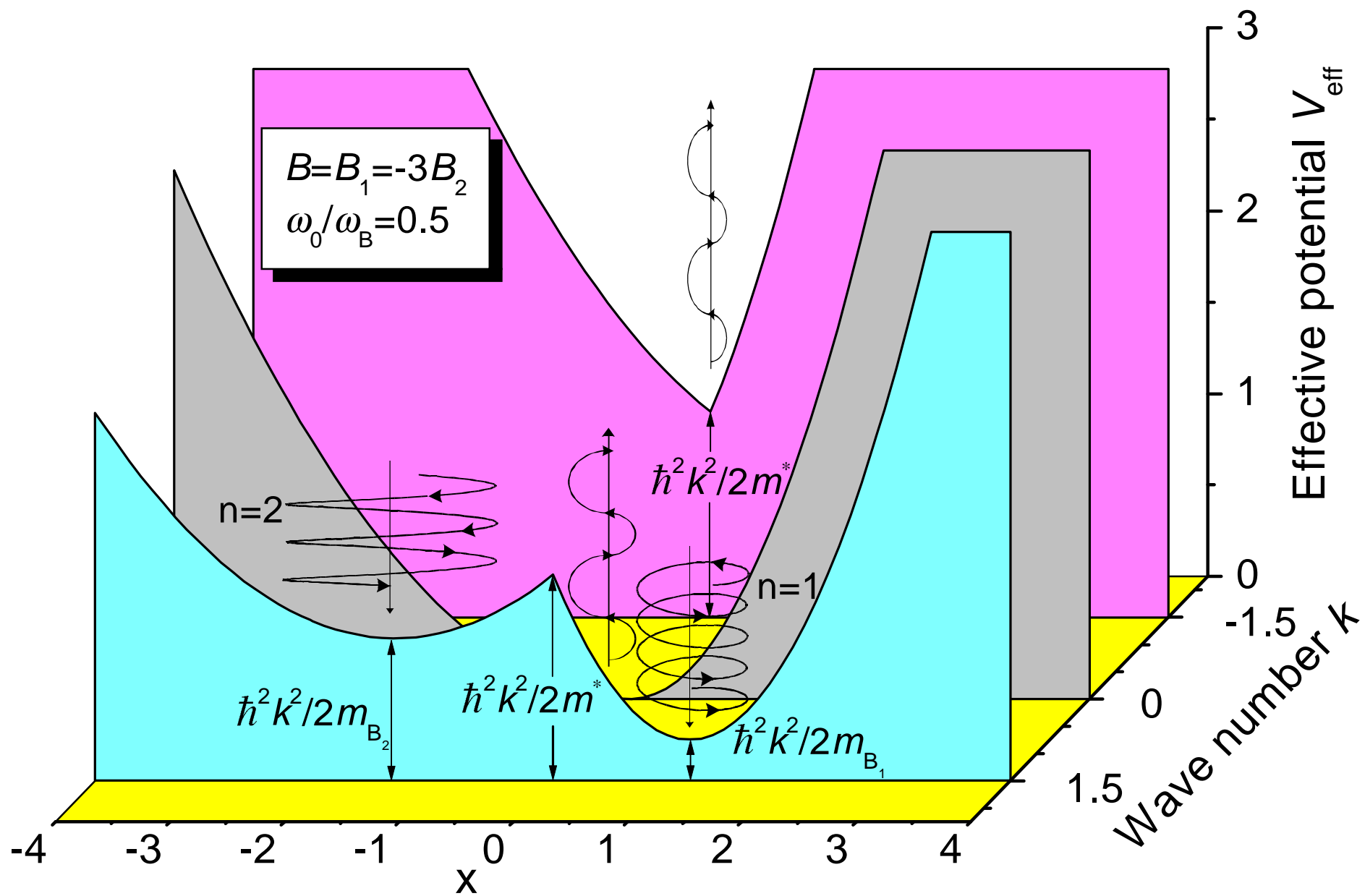
FIG. 19. Dependence of the resistance, in units of $R_0 = \pi m^*l_0/(e^2\tau)$ with $l_0^2 = \hbar/(m^*\omega_0)$, on the background magnetic field in the diffusive regime for the $B_1 = -3B_2$ initial magnetic field profile and a fixed Fermi energy $E_F = 5\sqrt{5}\hbar\omega_0$. The resistance in the homogeneous magnetic field case is plotted for comparison.

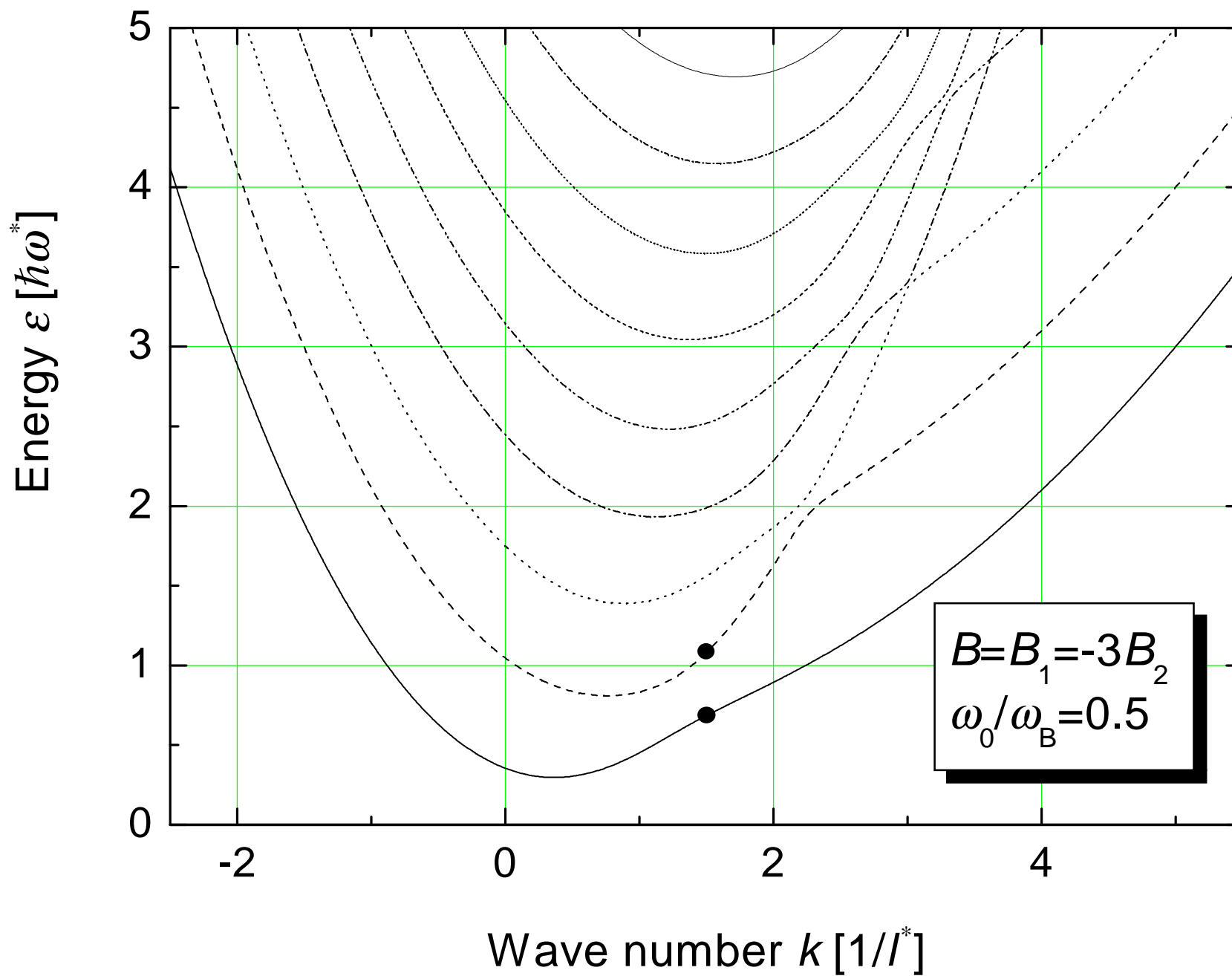


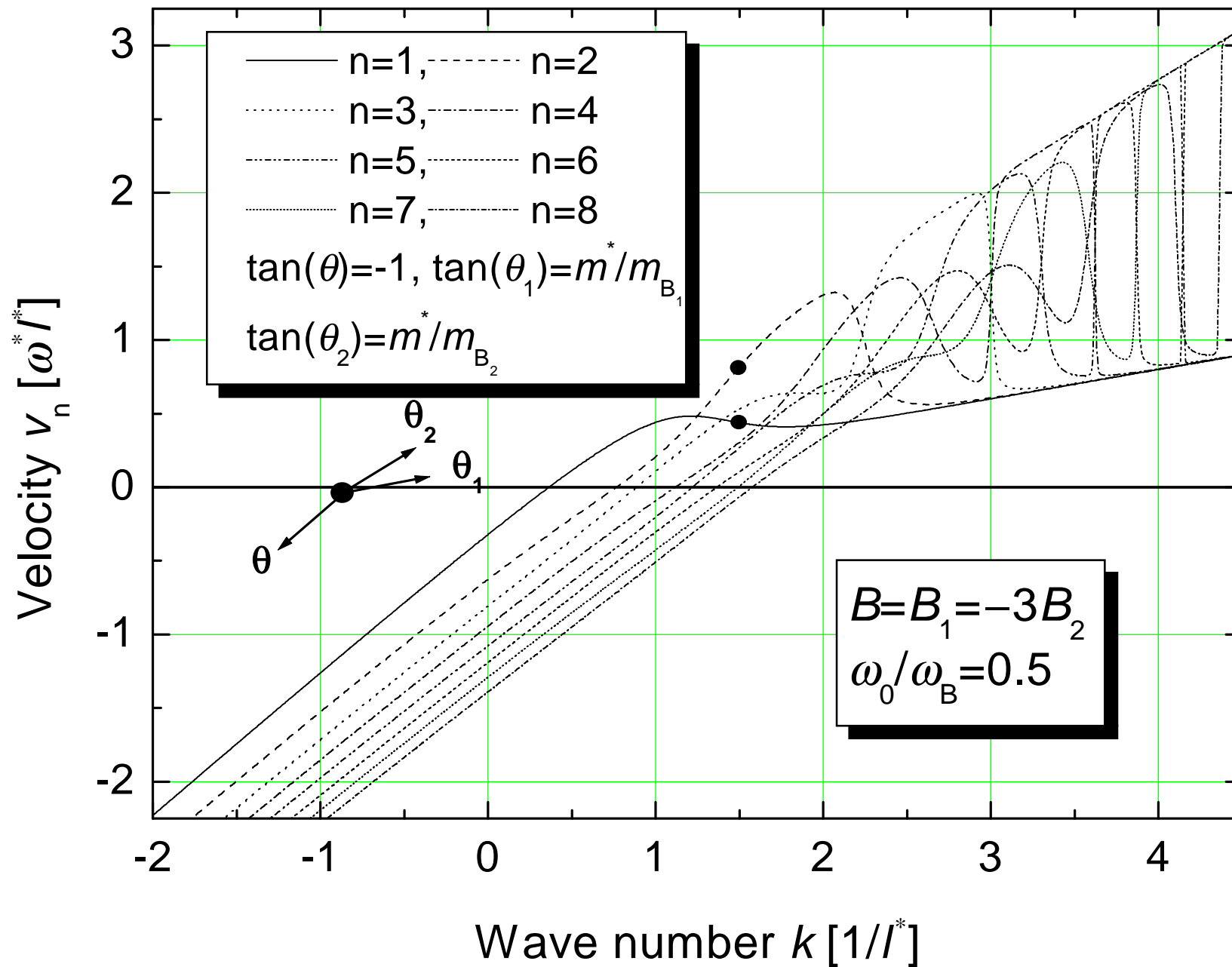


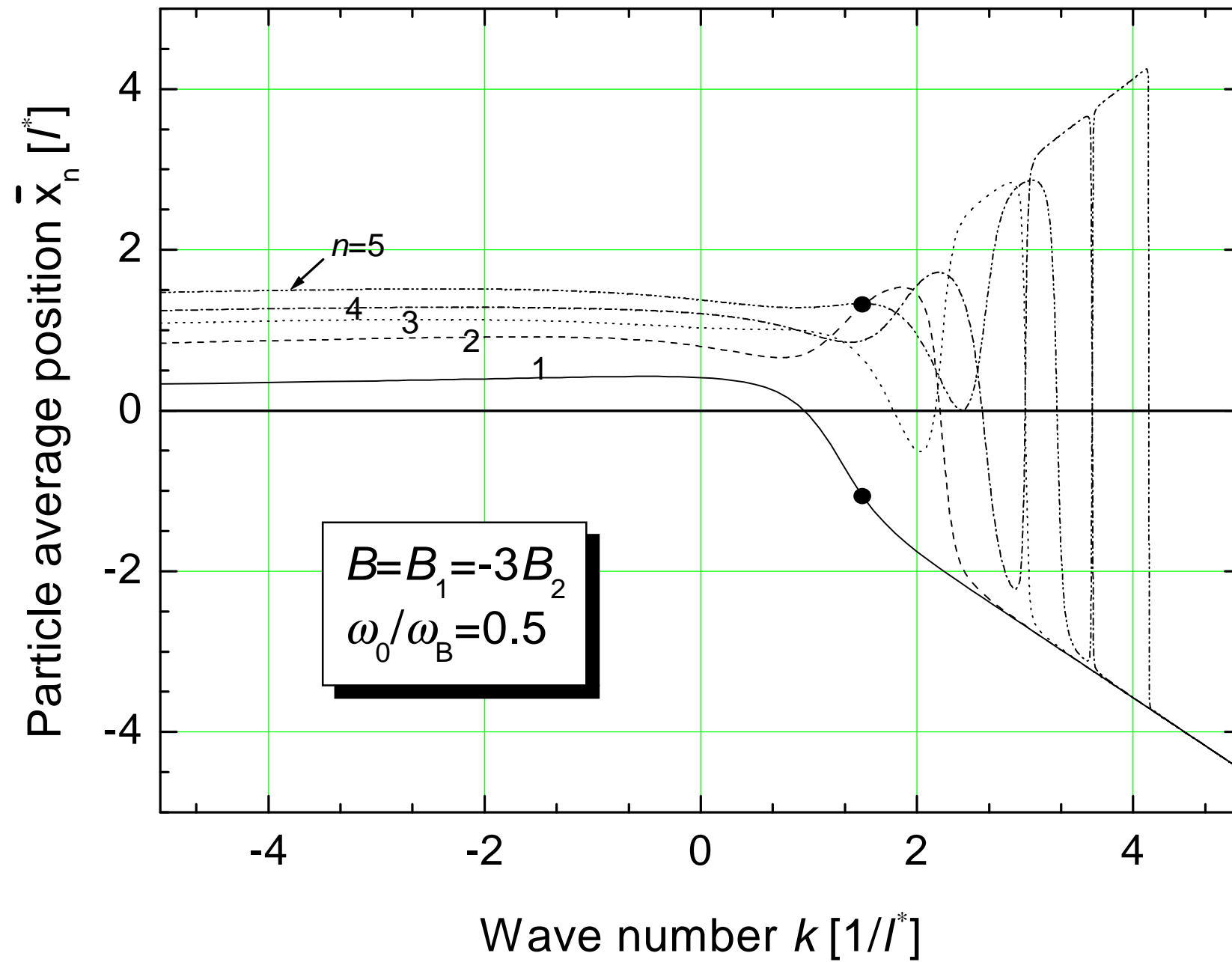


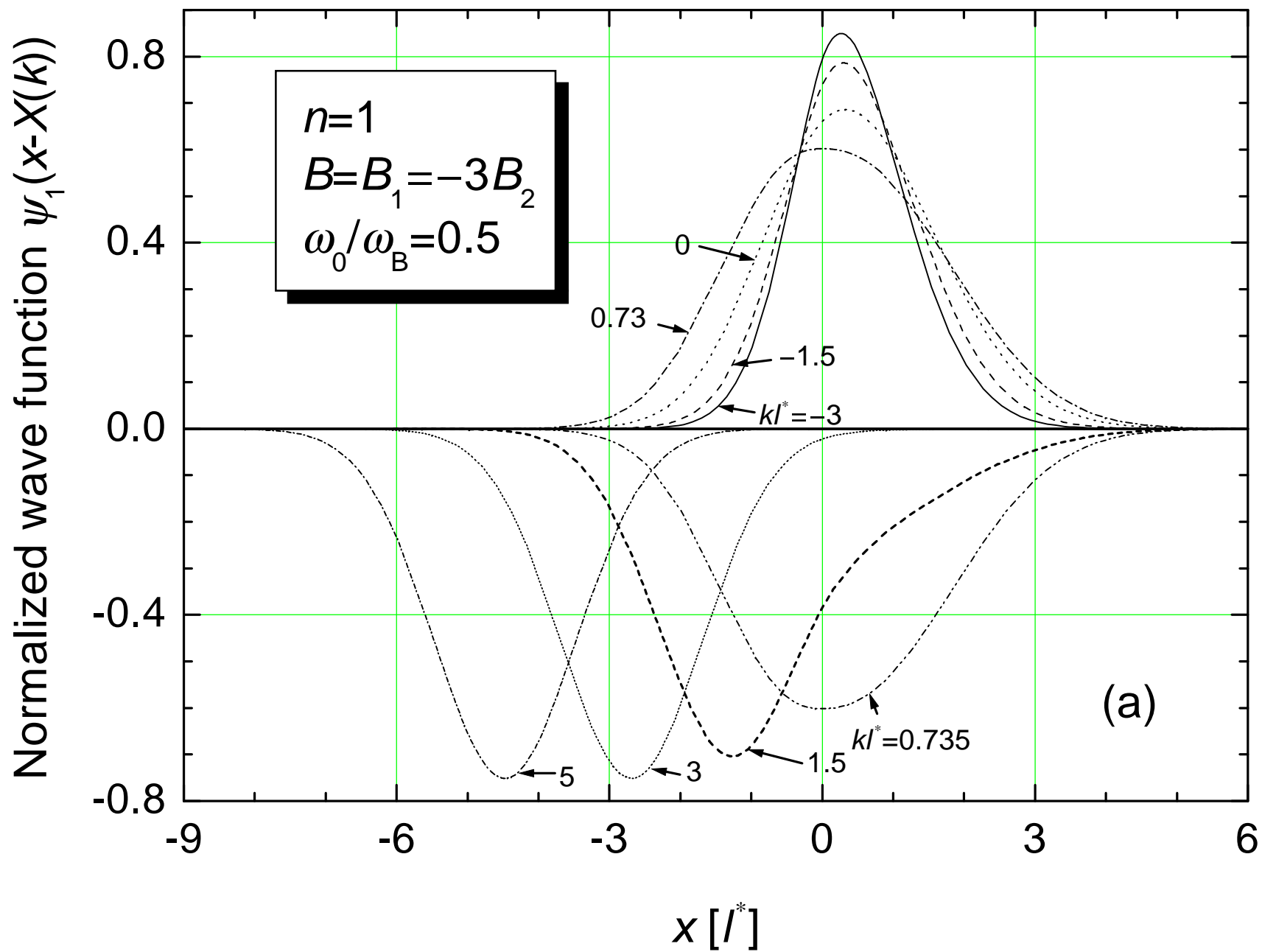












Normalized wave function $\psi_2(x-X(k))$

